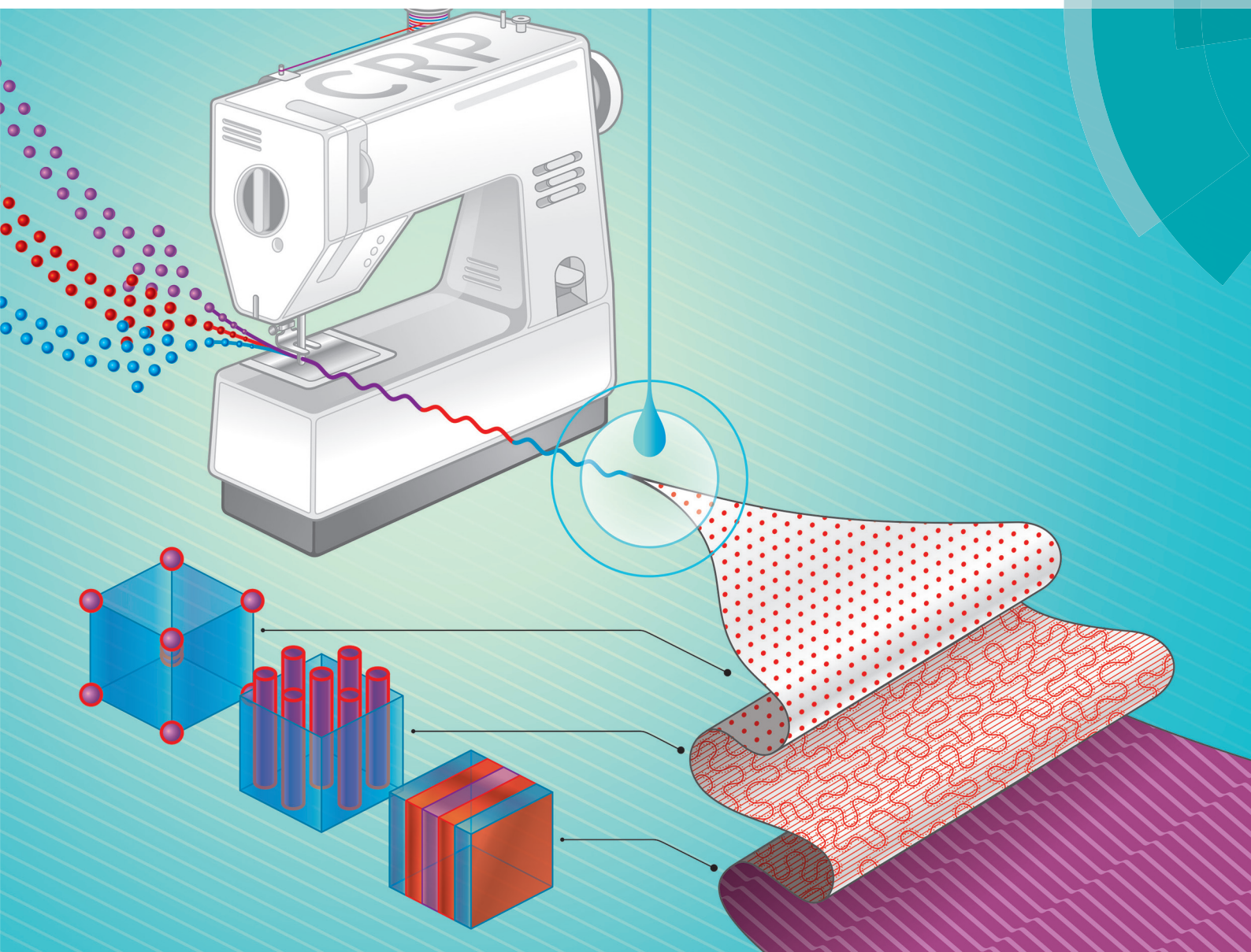


Polymer Chemistry

rsc.li/polymers

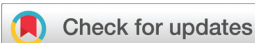


ISSN 1759-9962



PAPER

Chih-Feng Huang *et al.*
Synthesis of well-defined PCL-*b*-PnBA-*b*-PMMA ABC-type triblock copolymers: toward the construction of nanostructures in epoxy thermosets



Cite this: *Polym. Chem.*, 2018, **9**, 5644

Synthesis of well-defined PCL-*b*-PnBA-*b*-PMMA ABC-type triblock copolymers: toward the construction of nanostructures in epoxy thermosets†

Chih-Feng Huang, *^{a,b} Wen-Hua Chen,^a Junko Aimi, ^c Yi-Shen Huang,^a Sathesh Venkatesan,^a Yeo-Wan Chiang,^d Shih-Hung Huang,^d Shiao-Wei Kuo ^d and Tao Chen ^e

In this study we prepared a novel triblock copolymer (tBCP) through ring-opening polymerization (ROP) with ϵ -caprolactone (ϵ -CL) and two specific atom transfer radical polymerizations (ATRP), with *n*-butyl acrylate (nBA) and methyl methacrylate (MMA), respectively (herein, a supplemental activator and reducing agent and halogen-exchange ATRPs were employed). These chain-extending polymerizations were chosen to achieve controlled/living polymerization. This strategy afforded a well-defined ABC-type PCL-*b*-PnBA-*b*-PMMA tBCP ($M_{n, GPC} = 56\ 600$; PDI = 1.18) comprising two external miscible blocks with an epoxy monomer and a middle soft block. After curing with the diglycidyl ether of bisphenol-A and 4,4'-methylenedianiline, the miscibility of the resulting epoxy thermoset (ET)/tBCP composites was examined using Fourier transform infrared spectroscopy, differential scanning calorimetry, and thermogravimetric analysis. On further examining the ET/tBCP microstructures using transmission electron microscopy and small-angle X-ray scattering, we observed transitions with a long range order—from lamellar to core/shell cylinder to short core/shell cylinder morphologies—upon increasing the amount of ET. The domain sizes obtained after the curing reaction were in the range of approximately 30–60 nm.

Received 18th September 2018,
Accepted 6th November 2018

DOI: 10.1039/c8py01357h

rsc.li/polymers

1. Introduction

The construction of nanostructures within thermosetting resins, including epoxies,^{1–6} phenolics,^{7–12} and polybenzoxazines,^{13–17} has attracted great interest in fundamental research and industrially because of their potential applications in mesoporous materials, catalysts, separations, lithography, and shape memory materials, as well as the prac-

tical preparation of toughened materials. There are two mechanisms—self-assembly (SA) and reaction-induced microphase separation (RIMPS)—that have been used to access spherical, worm-like, lamellar, and vesicle nanostructures in thermoset matrices.^{3,18} Bates *et al.* were the first to create nanostructures in epoxy thermoset (ET) blends, using ET/amphiphilic diblock copolymers (diBCPs).^{3,4} They investigated the blends formed from diglycidyl ether of bisphenol-A (DGEBA) with poly(ethylene oxide)-*b*-poly(ethyl ethylene) (PEO-*b*-PEE) and poly(ethylene oxide)-*b*-poly(ethylene-*alt*-propylene) (PEO-*b*-PEP) diBCPs. Through an SA mechanism, they obtained long-range-ordered structures on the scale of nanometers through intermolecular interactions and observed a variety of transitions based on the blending compositions and extent of epoxy conversion. Bates *et al.* also prepared various composite systems upon introducing glycidyl groups into BCPs.^{5,19–23} Through chemical reactions between ETs and BCPs, the glycidyl methacrylate-containing BCPs could, therefore, undergo even curing within the epoxy matrix. They also investigated several reactive BCPs to induce microphase separation in the ET matrix.^{24–28} Among these reactive blend systems, however, only a limited number featured highly long-range-ordered nanostructures in the

^aDepartment of Chemical Engineering, National Chung Hsing University, 145 Xingda Road, Taichung 402-27, Taiwan. E-mail: HuangCF@dragon.nchu.edu.tw

^bResearch Center for Sustainable Energy and Nanotechnology, National Chung Hsing University, 145 Xingda Road, Taichung 402-27, Taiwan

^cMolecular Design & Function Group, Research Center for Functional Materials, National Institute for Materials Science, 1-2-1 Sengen, Tsukuba, Ibaraki 305-0047, Japan

^dDepartment of Materials and Optoelectronic Science, Center for Nanoscience and Nanotechnology, National Sun Yat-Sen University, Kaohsiung 804-24, Taiwan

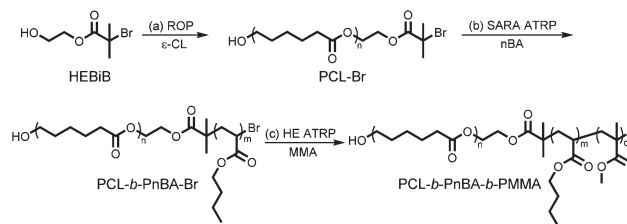
^eKey Laboratory of Bio-Based Polymeric Materials Technology and Application of Zhejiang Province, Ningbo Institute of Materials Technology and Engineering, Chinese Academy of Sciences, Ningbo 315201, China

† Electronic supplementary information (ESI) available. See DOI: 10.1039/c8py01357h

ETs,^{19,23,26,27} presumably because of rapid loss of the subtle interplay among the attractive (ξ) and repulsive (χ) forces between the ET and the reactive BCP.

Enormous numbers of diBCPs have been synthesized as modifiers to examine the phase separation within ETs.^{18,29–39} Several researchers have obtained many appealing long-range-ordered nanostructures by exploiting competitive intermolecular interactions (*i.e.*, hydrogen bonding and/or π - π interactions), including ET/poly(ethylene oxide)-*b*-polystyrene (PEO-*b*-PS)¹⁸ and ET/poly(2-vinylpyridine)-*b*-poly(ϵ -caprolactone) (P2VP-*b*-PCL)²⁹ systems. In addition, some ABA^{40–48} and ABC-type^{46,47,49–54} triblock copolymers (tBCPs) have been synthesized and examined for their compatibilities with ETs. For example, Ritzenthaler *et al.*^{49,50} prepared blends of ET/PS-*b*-PB-*b*-PMMA ABC-type tBCPs (PB: polybutadiene) that resulted in fascinating “raspberry-like” (sphere-on-sphere) and “onion-like” (multilayer) complex nanostructures. Using small-angle X-ray scattering (SAXS), Zheng *et al.* identified two imposing examples of ET/ABC-type tBCP blends—PDMS-*b*-PCL-*b*-PS (PDMS: polydimethylsiloxane)⁵¹ and PS-*b*-PCL-*b*-PnBA [PnBA: poly(*n*-butyl acrylate)]⁵²—featuring long-range-ordered nanostructures, prepared through the dual RIMPS mechanism. Nevertheless, examples of the construction of long-range-ordered nanostructures within an ET matrix using ABC-type tBCPs have remained limited.

Living polymerizations are powerful tools that provide access, using a variety of functional monomers, to polymers with predictable/controllable molecular weights (MWs) and narrow molecular weight distributions (MWDs).^{55–60} Well-known living polymerizations include anionic^{61–63}/cationic^{64–66} polymerizations, reversible-deactivation radical polymerizations [RDRPs;^{67–72} commonly, atom transfer radical polymerization (ATRP), reversible addition–fragmentation chain transfer (RAFT) polymerization, and nitroxide-mediated polymerization (NMP)], ring-opening (metathesis) polymerization [RO(M)P],^{73,74} and the newly developed chain-growth condensation polymerization (CGCP).⁷⁵ Among the diverse ATRP systems, two specific polymerization techniques are notable. First, the supplemental activator and reducing agent (SARA) ATRP technique allows living polymerizations to be performed with the aid of a zerovalent metal (*e.g.*, Cu⁰, Zn⁰, Mg⁰, or Fe⁰).^{76–78} In the presence of a zerovalent metal, a ppm-level of copper halide can be used to synthesize various homopolymers and BCPs. Second, the halogen exchange (HE) ATRP technique dictates the occurrence of the HE reaction by using a mixed-halide system (*e.g.*, a R–Br/CuCl system) that results in an increase in the initiation rate and a decrease in the propagation rate, relatively.⁷⁹ Representative examples include the chain extensions of PnBA–Br in the synthesis of PnBA-*b*-PMMA (star) BCPs, where the PnBA blocks are prepared first and then the PMMA is grown from the bromide ends using CuCl.^{80,81} This HE ATRP can effectively overcome the difficulty of chain extension from the macroinitiator (MI) with a less active chain end to the more reactive monomer, and leads to a controlled/living polymerization. Using the aforementioned



Scheme 1 Synthesis of the PCL-*b*-PnBA-*b*-PMMA tBCP through (a) ROP and (b and c) sequential ATRPs.

tools, one can apply a variety of approaches—such as a single polymerization method, or combinations of at least two polymerization methods, or even involve other effective reactions (*e.g.*, “click” chemistry)—to achieve the synthesis of well-defined ABC-type tBCPs.

Our purpose for this study was to design a novel ABC-type tBCP and explore its effectiveness at constructing nanostructures in an ET. As displayed in Scheme 1a, we employed low-temperature ROP of a bifunctional initiator (HEBiB) with ϵ -caprolactone (ϵ -CL), mediated by an organocatalyst (diphenyl phosphate), to synthesize the PCL–Br macroinitiator (MI). Then, we used SARA ATRP for the chain extension of the PCL–Br MI with nBA to obtain the PCL-*b*-PnBA–Br diBCP (Scheme 1b). Thereafter, we employed HE ATRP (Scheme 1c) to overcome the challenge of the chain extension of PCL-*b*-PnBA–Br with methyl methacrylate (MMA). These chain extension polymerizations were traced to examine their kinetics of living polymerization. A well-defined ABC-type tBCP, PCL-*b*-PnBA-*b*-PMMA, was eventually obtained, featuring two external miscible blocks with an epoxy monomer and a middle soft block. We further examined the compatibility of the ET/tBCP using Fourier-transform infrared (FT-IR) spectroscopy, differential scanning calorimetry (DSC), thermogravimetric analysis (TGA), wide-angle X-ray scattering (WAXS), transmission electron microscopy (TEM), and small-angle X-ray scattering (SAXS).

2. Experimental

2.1. Materials

Copper powder (Cu, 99.5%, 150 mesh), copper(II) bromide (CuBr₂, 99%), copper(II) chloride (CuCl₂, 97%), *N,N,N',N',N'*-pentamethyldiethylenetriamine (PMDETA), alumina (neutral), *n*-butyl acrylate (nBA, 98%), the epoxy monomer diglycidyl ether of bisphenol-A [DGEBA (epoxy equivalent weight = 189)], 4,4'-methylenedianiline (MDA, 98%), and methyl methacrylate (MMA, 99%) were purchased from Sigma–Aldrich. 2-Bromoisobutyl bromide (BiB, 97%), ethylene glycol (EG, 99%), ϵ -caprolactone (ϵ -CL (98%), triethylamine (TEA, 99.5%), and diphenyl phosphate (DPP, 97%) were purchased from Acros. 2-Hydroxyethyl 2-bromoisobutyrate (HEBiB) was synthesized from BiB and EG according to previously reported procedures.^{82,83} All solvents and monomers were purified and stored over molecular sieves prior to use.

2.2. ROP of HEBiB with ϵ -CL (*i.e.*, Scheme 1a)

The HEBiB initiator (0.21 g, 1 mmol), freshly distilled ϵ -CL monomer (16.5 mL, 150 mmol), and DPP catalyst (0.25 g, 1 mmol) were mixed in a Schlenk flask in the presence of a small amount of anhydrous toluene as the internal standard. The reaction mixture was kept at 40 °C in an oil bath for a desired period under $N_{2(g)}$ and the conversion of the ϵ -CL monomer was monitored using gas chromatography (GC). After the reaction had completed, the mixture was diluted with THF and twice-precipitated into cold MeOH. The white powder was collected and dried in a vacuum oven to obtain PCL-Br MI ($M_{n, NMR} = 12\ 080$, $M_{n, GPC} = 15\ 800$, PDI = 1.15; yield 69%).

2.3. Sequential SARA and HE ATRPs (*i.e.*, Scheme 1b and c)

For the SARA ATRP: PCL-Br MI (1.62 g, 0.100 mmol), nBA (7.20 mL, 50.0 mmol), Cu powder (8.3 mg, 0.13 mmol), CuBr₂ (15 mg, 0.07 mmol), PMDETA (42 μ L, 0.20 mmol), and anisole (7.2 mL) were added to a Schlenk flask ($[nBA]_0 = 3.47$ M), with anisole as the internal standard. The sealed flask was treated to three freeze/pump/thaw cycles to remove O₂. The flask was immersed in a thermostatted bath at 100 °C and then samples were withdrawn after appropriate periods. The conversion of the monomer and the molecular weight (MW) of the polymer were confirmed using GC and gel permeation chromatography (GPC), respectively. When completed, the reaction mixture was quenched with ice and exposed to air. The mixture was diluted with THF, passed through alumina (neutral), and precipitated into cold MeOH. The sediment was collected and dried in a vacuum oven overnight to obtain PCL-*b*-PnBA-Br MI ($M_{n, NMR} = 34\ 130$; $M_{n, GPC} = 42\ 000$; PDI = 1.12; yield 50%). For HE ATRP: The obtained PCL-*b*-PnBA-Br MI (4.0 g, 0.090 mmol), MMA (4.0 mL, 36 mmol), Cu powder (7.4 mg, 0.12 mmol), CuCl₂ (8.5 mg, 0.063 mmol), PMDETA (37 μ L, 0.18 mmol), and anisole (12 mL) were added to a Schlenk flask ($[MMA]_0 = 2.25$ M) and subjected to a procedure similar to that of the SARA ATRP. After degassing, the flask was heated at 80 °C. After the reaction had reached completion, similar purification steps were applied to obtain the PCL-*b*-PnBA-*b*-PMMA tBCP ($M_{n, NMR} = 46\ 730$; $M_{n, GPC} = 56\ 600$; PDI = 1.18; yield 70%) excepting that the resultant product was precipitated into MeOH at room temperature (~ 28 °C) to remove the unreacted diBCP. From nuclear magnetic resonance (NMR) spectral data, the volume fractions (f) of the tBCP were as follows: $f_{PCL} = 0.25$; $f_{PnBA} = 0.46$; and $f_{PMMA} = 0.29$ [$\rho_{(PCL)} = 1.145$; $\rho_{(PnBA)} = 1.08$; $\rho_{(PMMA)} = 1.18$; and $\rho_{(ET)} = 1.15$].

2.4. ET/tBCP composites

The epoxy monomer DGEBA and the tBCP were mixed at various weight ratios and then heated at 100 °C to form homogeneous mixtures. A stoichiometric amount of an epoxy curing agent, MDA, was added to each mixture, which was then transferred to an alumina pan. The curing reactions were performed at 150 °C for 12 h. The samples were subjected to further post-curing reactions at 180 °C for 2 h to obtain the ET/tBCP composites.

2.5. Characterization

Analytical GPC, using two PSS SDV columns (Linear S and 100 Å pore size), a Waters 515 pump, and a Waters 410 differential refractometer, was performed at 40 °C (eluent: THF; flow rate: 1 mL min⁻¹). A calibration curve, from a set of polystyrene standards with different molecular weights and narrow molecular distributions, was prepared to characterize the samples in terms of their values of M_n , M_w , and M_w/M_n (*i.e.* PDI). Proton (¹H) nuclear magnetic resonance spectra were recorded using a Varian 400 NMR and calibrated using an internal standard of CDCl₃ ($\delta = 7.26$ ppm). FT-IR spectra were recorded using a Nicolet Avatar 320 FT-IR spectrometer operated at a resolution of 4 cm⁻¹, with 64 scans. The samples were dissolved in THF and cast on a KBr plate. The vacuum-dried samples were charged into a N₂-purged chamber to maintain environmental dryness. The glass transition temperatures (T_g) of the polymers were analyzed under N₂ using a Seiko 6220 differential scanning calorimeter (first run: 5 min isothermal at 200 °C and quenching of the samples using liquid N₂; second run: ramping at 20 °C min⁻¹ from -80 to +190 °C). TGA of the composites was performed using a TA Instruments Q50 analyzer featuring a platinum holder (ramping: 20 °C min⁻¹; range: 50–700 °C; under N_{2(g)}). TEM images were recorded using a JEOL JEM-2100 transmission electron microscope operated at an accelerating voltage of 200 kV. The thin film of the pure tBCP sample was prepared using a cryomicrotome; thin films of the composite samples were prepared by microtoming under ambient conditions. All TEM samples were stained with RuO₄. SAXS was performed using the Endstation BL23A1 of the National Synchrotron Radiation Research Center (NSRRC), Hsinchu, Taiwan. The sample-to-detector distance and the energy of the X-ray source were 3 m and 15 kV, respectively. The scattering profile collected by using a Pilatus-1MF detector was plotted in terms of the scattering intensity (I) with respect to the magnitude of the scattering vector [$q = (4\pi/\lambda)\sin(\theta/2)$]. The d -spacings were estimated from the first-order scattering peaks (q^*), using the formula $d = 2\pi/q^*$. WAXS was performed, over diffraction angles (2θ) from 3 to 50°, using an X-ray diffractometer (Bruker AXS D8 Discover SSS high-resolution) and Ni-filtered CuK α radiation ($\lambda = 1.54$ Å) at 50 kV and 50 mA.

3. Results and discussion

3.1. Synthesis and characterization of (block co)polymers

The non-toxic and chemically stable compound DPP can be an efficient organocatalyst for ROP at low temperature.^{84–86} We can expect that it could provide mild reaction conditions, leading to preservation of the functionality of our bifunctional initiator during polymerization. Through the ROP of the bifunctional initiator HEBiB with the monomer ϵ -CL (ϵ -CL/HEBiB/DPP = 200/1/1 at 40 °C; $[\epsilon\text{-CL}]_0 = 9.0$ M), we obtained the PCL-Br MI ($M_{n, GPC} = 15\ 800$; PDI = 1.15). As revealed from the peak area ratio of (b'/6H)/(a'/2H) in the ¹H NMR spectrum in Fig. S1 (ESI[†]), we obtained a PCL having a number-average

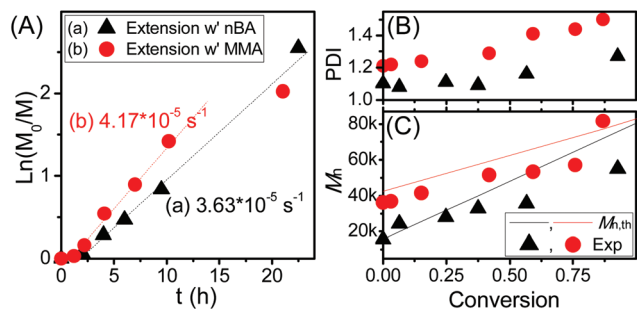


Fig. 1 Kinetic plots of chain extensions *via* ATRP of (triangles) PCL–Br with nBA and (circles) PCL-*b*-PnBA–Br with MMA, corresponding to the preparations of the di- and triblock copolymers.

molecular weight ($M_{n, \text{NMR}}$) of 12 080 (*i.e.*, $n = ca.$ 104), with high chain-end integrity of the tertiary bromoester. Namely, the terminal groups are present in approximately equal amounts within experimental error. The well-defined PCL–Br MI was then used in subsequent chain extensions with nBA and MMA. The data (triangles) in Fig. 1 represent kinetic plots of the first chain extension with nBA *via* SARA ATRP, which has been demonstrated as an effective controlled/living radical polymerization tool in the presence of a small number of catalysts. For the chain extension with nBA *via* SARA ATRP (nBA/PCL–Br/Cu⁰/CuBr₂/PMDETA = 500/1/1.3/0.7/2 at 100 °C; [nBA]₀ = 3.47 M), the triangles in Fig. 1A reveal a linear first-order plot and an apparent rate constant (k_{app}) of approximately $3.63 \times 10^{-5} \text{ s}^{-1}$. In Fig. 1B and C, the values of the triangles for the molecular weight distribution (*i.e.*, PDI) were less than 1.30, and the evolution of the number-average molecular weight revealed linear growth. The GPC traces in Fig. 2A reveal the gradual increases in the MWs with low PDIs within less than 10 h. A long reaction time of 24 h might cause some side reactions (*e.g.*, termination in coupling or a chain transfer reaction), as evidenced by a shoulder in the GPC traces.

Accordingly, we prepared a well-defined diblock MI (*i.e.*, PCL-*b*-PnBA–Br: $M_{n, \text{GPC}} = 42\,000$; PDI = 1.12) for the second

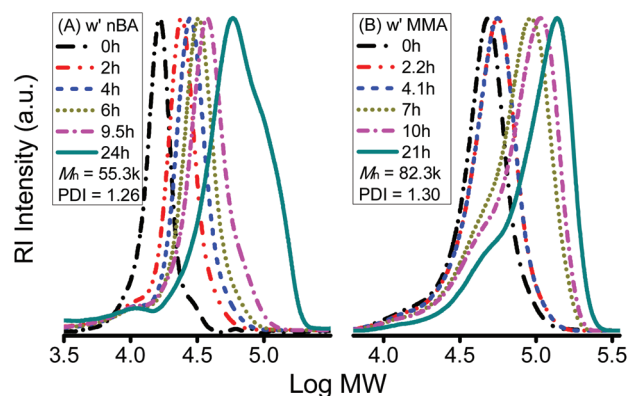


Fig. 2 GPC traces for the chain extensions of (A) PCL–Br with nBA and (B) PCL-*b*-PnBA–Br with MMA, for the syntheses of the PCL-*b*-PnBA and PCL-*b*-PnBA-*b*-PMMA BCPs, respectively.

chain extension with MMA, using HE ATRP, which can overcome the problem of radical reactivity between methacrylates and acrylates during polymerization. In general, the activity of a secondary bromoester of a PCL-*b*-PnBA–Br MI chain end is approximately 10 ten times lower than that of a tertiary bromoester presented during the chain extension with MMA. This phenomenon should lead to a poor chain extension product, providing a bimodal and broadened molecular weight distribution. By taking advantage of the HE ATRP, as displayed in Scheme S1,[†] the mixed halide system could guide the chain extension of PCL-*b*-PnBA–Br with MMA in a controlled manner through mediation of the activity at the chain end. The activation rate constants (k_{act}) of chlorine-based initiators have *ca.* an order less than those of bromine-based initiators.⁸⁷ For the chain extension with MMA through HE ATRP (MMA/PCL-*b*-PnBA–Br/Cu⁰/CuCl₂/PMDETA = 400/1/1.3/0.67/2 at 80 °C; [MMA]₀ = 2.25 M), the circles in Fig. 1A reveal a linear first-order plot prior to 10 h and an apparent rate constant (k_{app}) of approximately $4.17 \times 10^{-5} \text{ s}^{-1}$. A deviation from the linear-fitting curve was obtained because of some side reactions at a higher conversion of MMA. As displayed in Fig. 1B and C, the PDIs of the circle data were less than 1.5, and the evolution of the value of M_n occurred with linear growth prior to 10 h. We ascribe the deviation from the theoretical molecular weight line (*i.e.*, $M_{n, \text{th}}$) to hydrodynamic differences among the polystyrene standards and the tBCPs. From the GPC traces in Fig. 2B, the trend in the growth of the MWs revealed a narrow molecular weight distribution.

The chemical structures of the homo- and block copolymers were analyzed using NMR spectroscopy. Fig. 3 presents the ¹H NMR spectra of (A) PCL, (B) PCL-*b*-PnBA, and (C) PCL-*b*-PnBA-*b*-PMMA, with their representative peaks assigned. In Fig. 3A, peaks a–d, located near 4.06, 2.30, 1.64, and 1.37 ppm, represent the PCL chain. After the chain extension with nBA, we observed broadening of several peaks, including (a + e),

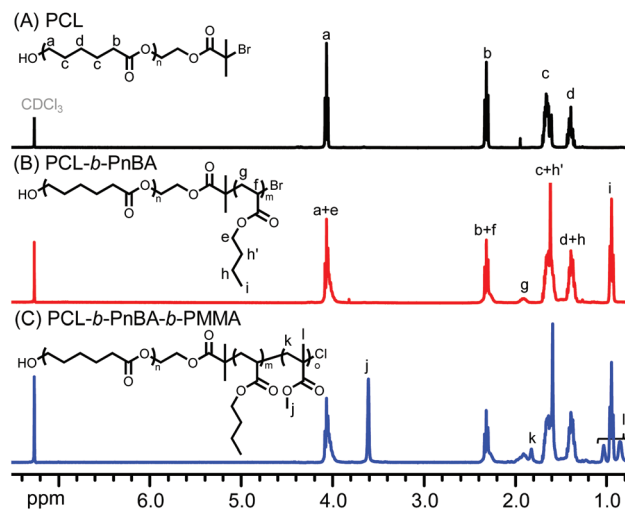


Fig. 3 ¹H NMR spectra (400 MHz, CDCl₃) of (A) PCL, (B) PCL-*b*-PnBA, and (C) PCL-*b*-PnBA-*b*-PMMA (block co)polymers.

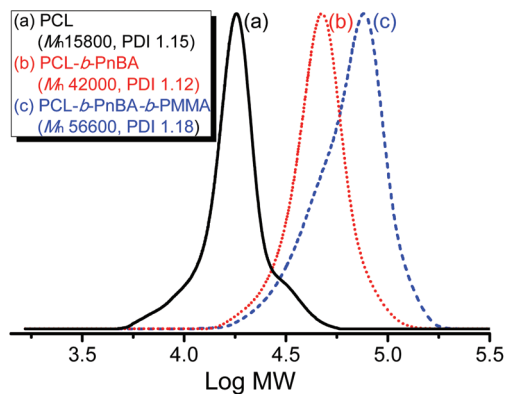


Fig. 4 GPC traces of the obtained (a) PCL, (b) PCL-*b*-PnBA, and (c) PCL-*b*-PnBA-*b*-PMMA (block co)polymers.

(*b* + *f*), (*c* + *h*'), and (*d* + *h*), as well as additional peaks *g* and *i* (*ca.* 1.90 and 0.93 ppm), as displayed in Fig. 3B. From the chain extension data in Fig. 1, 2A, and 3B, we confirmed that we had successfully obtained well-defined PCL-*b*-PnBA diBCPs. As presented in Fig. 3C, broadening of the peaks occurred and the additional peaks *j*, *k*, and *l* (*ca.* 3.60, 1.81, and 1.01/0.83 ppm) appeared after the chain extension with MMA. The chain extension data in Fig. 1, 2B, and 3C confirm that a well-defined ABC-type tBCP ($M_{n, \text{NMR}} = 46\,730$; $M_{n, \text{GPC}} = 56\,600$; PDI = 1.18) had been obtained. Fig. 4 and S2† provide analyses of the GPC and FT-IR spectra of the resulting BCPs. We could slightly observe a shoulder in the GPC trace of Fig. 4c; however, we carried out the precipitation of the ABC tBCP in MeOH at room temperature which can easily remove the PCL-*b*-PnBA diBCP. Thus the shoulder presumably resulted from the original difficulty of chain extension of a polyacrylate MI with methacrylate monomers. Table 1 summarizes the reaction conditions of the well-defined (co)polymerizations.

3.2. Phase separation mechanism and hydrogen bonding interactions between ET and tBCP

The obtained PCL₁₀₄-*b*-PnBA₁₇₂-*b*-PMMA₁₂₆ tBCP was further used to blend with the ET cured from DGEBA and MDA. The

Table 1 Reaction conditions and characterization of the resulting (co) polymers

Entry ^a	Monomer	[M]	Temp. (°C)	$M_{n, \text{GPC}}^b$	PDI ^b	$M_{n, \text{NMR}}^c$
1	ε-CL	9.0	40	15 800	1.15	12 080
2	nBA	3.47	100	42 000	1.12	34 130
3	MMA	2.25	80	56 600	1.18	46 730

^a 1: ε-CL/HEBiB/DPP = 200/1/1 for ROP; 2: nBA/PCL-Br/Cu⁰/CuBr₂/PMDETA for the first chain extension; 3: MMA/PCL-*b*-PnBA-Br/Cu⁰/CuCl₂/PMDETA = 400/1/1.3/0.67/2 for the second chain extension.

^b Characterized through GPC (eluent: THF; flow rate: 1 mL min⁻¹; 35 °C), based on monodisperse polystyrene standards. ^c The corresponding resultants to entries are PCL₁₀₄, PCL₁₀₄-*b*-PnBA₁₇₂, and PCL₁₀₄-*b*-PnBA₁₇₂-*b*-PMMA₁₂₆, characterized using ¹H NMR spectroscopy, where the subscripts represent the number of repeating units.

miscibility of ET/ABC-type tBCP blends resulted in the following factors: (i) the PCL segment is miscible with the epoxy monomer and miscible or at least partially miscible with the ET,^{88–90} (ii) the PMMA segment is miscible with the epoxy monomer but undergoes reaction-induced phase separation during curing,^{91,92} and (iii) the PnBA segment is presumably immiscible with the epoxy monomer, but basically not with the ET.^{93,94} To confirm the phase separation mechanism, we conducted a SAXS measurement of a mixture of the epoxy monomer with MDA and tBCP (50 : 50, w/w) before and after curing. As revealed from curve a in Fig. 5, the microphase separation occurred through an SA mechanism prior to curing, suggesting that the PnBA segment was immiscible with the epoxy monomer and excluded out. Here, a presumably disordered spherical structure, having an average size of approximately 26 nm, was obtained. Curve b in Fig. 5 reveals that the microdomain was then re-organized through a RIMPS mechanism. A cylindrical structure (*i.e.*, q/q^* peaks with 1 : $\sqrt{3}$: $\sqrt{7}$) was formed, having a spacing of approximately 39 nm. We conclude that a two-stage phase separation process had occurred. The first stage of microphase separation occurred in the mixtures of epoxy monomer/tBCP, mainly the result of a thermodynamic SA mechanism. The second stage of structural reorganization was performed through an RIMP mechanism, majorly dominated by the kinetic curing process.

Before examining the microstructures of the blends, we analyze the interactions between the ET and the tBCP. We prepared ET/tBCP composites at various weight ratios, named herein tBCP70%-tBCP10%. Fig. 6 presents the FT-IR spectra of these ET/tBCP composites, namely in their OH (Fig. 6A) and C=O (Fig. 6B) spectral regions. Although the signal of the free

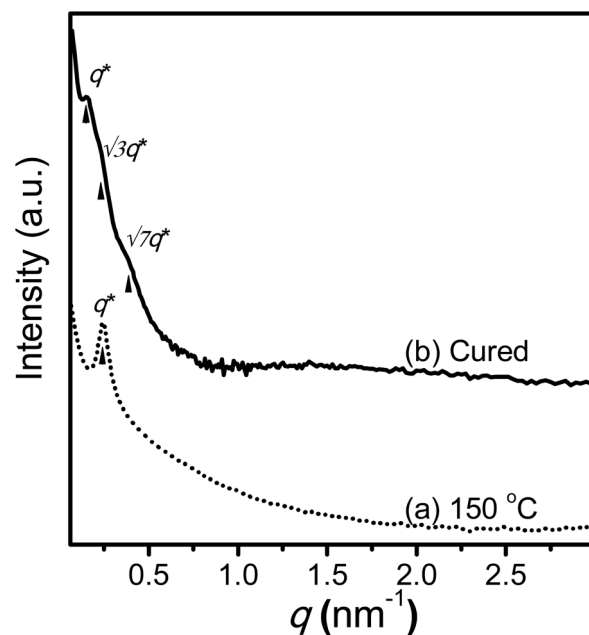


Fig. 5 SAXS profiles of a mixture of the epoxy monomer and tBCP (50 : 50, w/w), before and after curing.

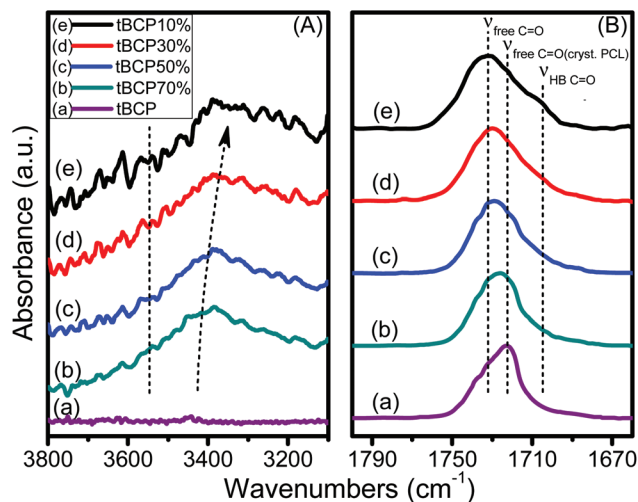


Fig. 6 FT-IR spectra of (a–e) ET/tBCP composites of various weight ratios, displaying the ranges (A) 3800–3100 and (B) 1800–1660 cm^{-1} .

OH groups remained almost stationary ($\nu = ca. 3510 \text{ cm}^{-1}$) in Fig. 6A, we observed a significant shift of the signal for the self-associated hydrogen-bonding (HB) OH groups (ν from $ca. 3400$ to 3330 cm^{-1}) upon increasing the amount of ET. The large wavenumber difference ($\Delta\nu$) between the signals for the free and HB OH groups indicated the great strength of the intermolecular HB between the ET and the tBCP. In the C=O region (Fig. 6B), three peaks could be assigned: free C=O groups from PMMA/PnBA/PCL ($\nu_{\text{free C=O}} = ca. 1734 \text{ cm}^{-1}$), the C=O groups from the crystalline PCL ($\nu_{\text{free C=O(cryst. PCL)}} = ca. 1724 \text{ cm}^{-1}$), and the HB C=O groups from PMMA and amorphous PCL ($\nu_{\text{HB C=O}} = ca. 1705 \text{ cm}^{-1}$). We detected an increase in intermolecular-associated HB among the OH and C=O groups from the PCL and PMMA blocks, consistent with the observations from the OH spectral region. These results indicated a weak hydrogen bonding among ET and both PCL and PMMA.

3.3. Thermal properties and crystallinity of the ET/tBCP composites

Fig. 7 presents DSC traces of the various samples. The pure tBCP (curve a) mainly featured a value of $T_{g, \text{PnBA}}$ ($ca. -44.8 \text{ }^\circ\text{C}$), a value of $T_{m, \text{PCL}}$ ($ca. 56.5 \text{ }^\circ\text{C}$), and a value of $T_{g, \text{PMMA}}$ ($ca. 106.6 \text{ }^\circ\text{C}$). The pure ET sample (curve f) had a value of T_g of approximately $150 \text{ }^\circ\text{C}$. For the composites (curves b–e), we noted three major characteristics: (i) a value of $T_{g, \text{PnBA}}$, (ii) the disappearance of the signal for $T_{m, \text{PCL}}$, and (iii) broadening of the higher single signal of T_g . In the higher- T_g region, notably, higher tBCP contents resulted in larger values of ΔT_g ($T_{g, \text{onset}} - T_{g, \text{end}}$). The three aforementioned characteristics corresponded to (i) an exclusive domain of the PnBA, (ii) a highly compatible domain comprising ET/PCL, and (iii) an inhomogeneous domain of ET/PMMA. In the composite with tBCP70% (curve b), a relatively large value of ΔT_g and a small peak for PCL melting (see inset) were obtained. The weak

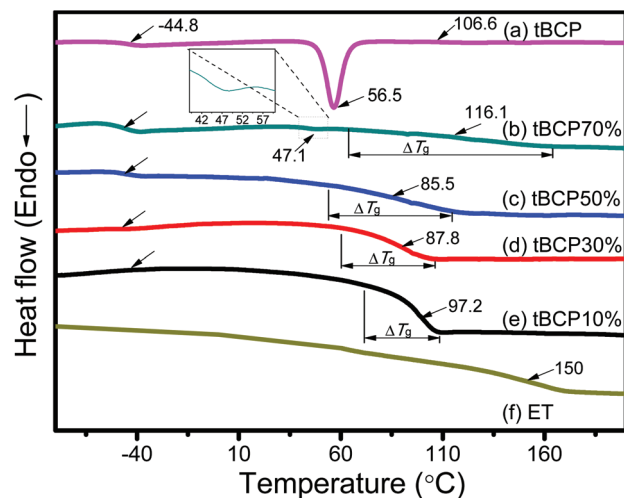


Fig. 7 DSC traces of ET/tBCP composites at various weight ratios.

intermolecular HB would presumably be insufficient to cause microphase separation within the composites. With the aid of the pre-formed SA nanostructures, however, the weak HB played a crucial role in the RIMPS process during the curing reaction. A similar phenomenon has been depicted in the previous literature.⁵⁴

The thermal stability of the ET/tBCP composites was investigated using TGA. As displayed in Fig. S3,† the tBCP (curve a) and the ET (curve f) mainly underwent single-step pyrolysis with a similar maximum decomposition rate (r_d) at approximately $400 \text{ }^\circ\text{C}$. Their thermal stabilities, based on 5 wt% weight loss temperatures ($T_{d5\%}$), were approximately 364 and $310 \text{ }^\circ\text{C}$, respectively, and their char yields were approximately 14.4 and $3.1 \text{ wt}\%$, respectively. For the composite samples (curves b–e), we obtained similar values of r_d , but all of the values of $T_{d5\%}$ (358 – $364 \text{ }^\circ\text{C}$) were higher than that of the pure tBCP, implying that the thermal stability remained after hybridization. The char yields were in a range of approximately 10 – $20 \text{ wt}\%$. These preliminary results indicated that ET/tBCP formed a highly compatible blending system at the nanoscale, and retained good thermal stability on the basis of the presence of neat ET. Table 2 summarizes the DSC and TGA data.

Table 2 Thermal properties of the ET/tBCP composites

Samples	T_g ($^\circ\text{C}$)	ΔT_g^a ($^\circ\text{C}$)	T_m ($^\circ\text{C}$)	$T_{d5\%}^b$ ($^\circ\text{C}$)	Char yield (%)
tBCP	-44.8, 106.6	—	56.5	310	3.1
tBCP70%	-46.6, 116.1	102.1	47.1	360	10.1
tBCP50%	-45.8, 85.5	60.7	—	358	12.8
tBCP30%	-47.3, 87.8	46.6	—	348	19.6
tBCP10%	-44.2, 97.2	37.7	—	348	20.6
ET	150	—	—	364	14.4

^a $\Delta T_g \equiv (T_{g, \text{onset}} - T_{g, \text{end}})$, determined from DSC traces of the higher- T_g regions. ^b $T_{d5\%}$: 5 wt% loss temperatures of the samples, determined from TGA profiles.

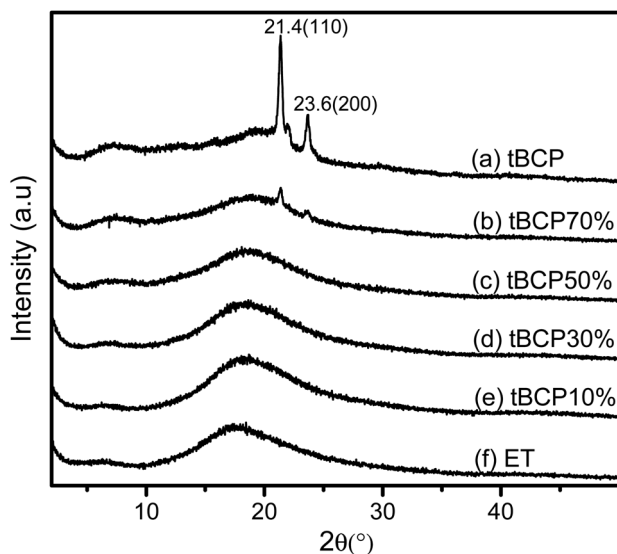


Fig. 8 WAXS analyses of ET/tBCP composites at various weight ratios.

Fig. 8 displays the WAXS data of the ET/tBCP composites. For the pure tBCP (curve a), the main diffraction peak at 21.4° correlated with a d -spacing of approximately 4.2 \AA , corresponding to the (110) plane of crystalline PCL, and the peak at 23.6° represented a d -spacing of approximately 3.8 \AA , corresponding to the (200) plane of the crystalline PCL.⁹⁵ For the composite tBCP70% (curve b), we observed not only amorphous peaks but also small crystalline peaks corresponding to the PCL segment. This finding suggested that tBCP70% possessed a slight excess of PCL chains that could form crystal micro-domains. These results are consistent with the DSC

data. For the composites tBCP50%, 30%, and 10% (curves c–e), we observed only peaks of amorphous halos, consistent with good miscibility between the ET and PCL segments, leading to suppression of PCL crystallization. For the pure ET (curve f), we observed only an amorphous halo pattern.

3.4. Microstructures of the ET/tBCP bulk

We examined the appearance of the ET/tBCP bulk films. Fig. S4† presents a photograph of broken ET pieces obtained after bending, illustrating the brittle mechanical properties of this material. Interestingly, the composites (*i.e.*, Fig. S4b–e†) exhibited good transparency and bendable mechanical properties (see inset images) for their thick films, indicating homogeneity. In the earlier DSC and WAXS measurements, we detected the existence of a PCL crystalline structure within the tBCP70% sample. We conclude that the PCL crystalline domain did not lead to macroscopic heterogeneity in the bulk material.

We then used TEM and SAXS to examine the morphology of microphase separation as shown in Fig. 9 and 10, respectively. For TEM analysis, the sections of pure tBCP were collected using a cryomicrotome with the aid of liquid N_2 and the sectioned composites were collected through microtoming under ambient conditions and images were collected at various magnifications in a bright-field mode. Prior to TEM measurements, all samples were stained with RuO_4 vapor to enhance the image contrast. Notably, the cured epoxy domains of the composites were much less stainable because of their highly crosslinked and dense structures.^{39,42,43} The microstructures of these composites were investigated through SAXS measurements which were performed at room temperature.

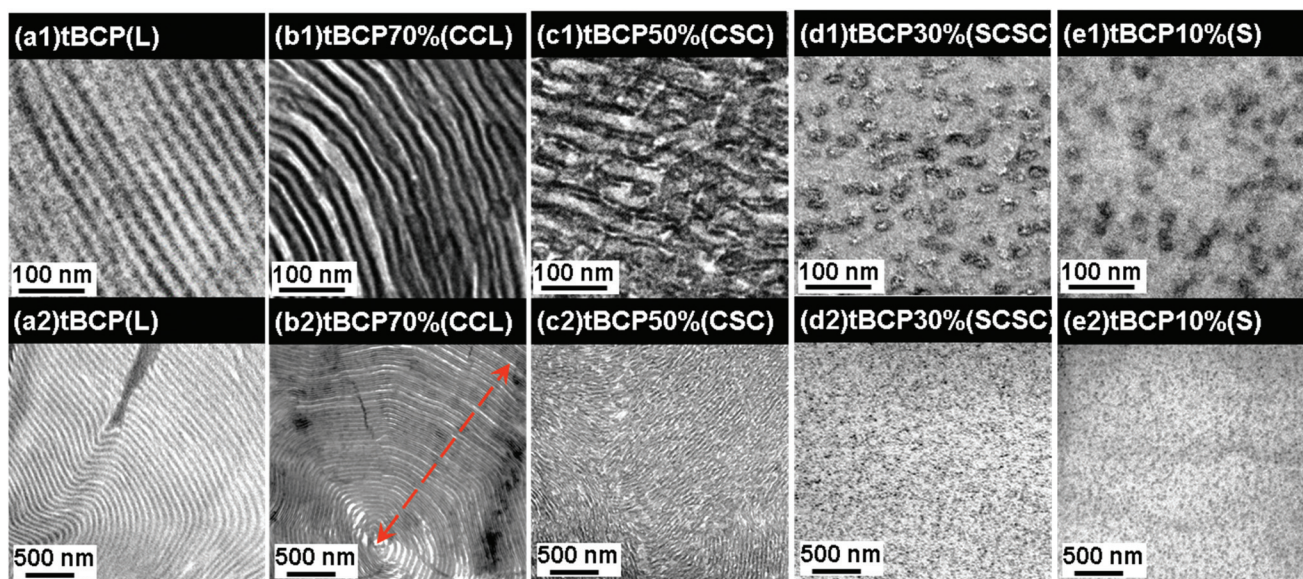


Fig. 9 TEM morphologies recorded over areas of approximately 0.4×0.4 and $2.5 \times 2.5 \mu\text{m}^2$ for the (1) and (2) series, respectively. (a–e) ET/tBCP composites at various weight ratios [sample (a): collected using a cryomicrotome; samples (b–e): stained with RuO_4 ; L: lamellae; CCL: concentric-circle lamellae; CSC: core/shell cylinder; SCSC: short core/shell cylinder; S: sphere].

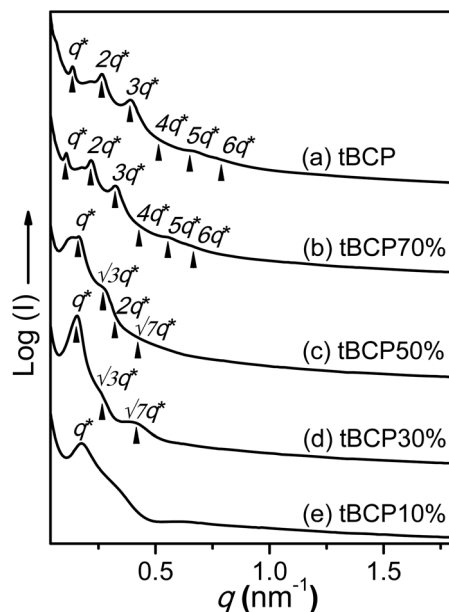


Fig. 10 SAXS profiles of ET/tBCP composites at various weight ratios.

Herein we concurrently discuss and comprehend the results of TEM (Fig. 9) and SAXS (Fig. 10). From the measurements of the pure tBCP in Fig. 9a and 10a, lamellar (L) morphology and the microstructure were obtained. In Fig. 9a, the ratio of dark regions in the lamellae structure matched the volume fraction of PnBA ($f_{\text{PnBA}} = ca. 0.46$) and alternating domains of each one of the blocks were clearly revealed. In Fig. 10a, we observed evidence for a long-range-ordered lamellar microstructure, corresponding to q/q^* peaks of 1:2:3:5 with a periodic size of approximately 46.5 nm. From the measurements of the tBCP70% composite in Fig. 9b and 10b, lamellar morphology and the microstructure were also obtained. In Fig. 9b, however, three-colored lamellar images were observed. The dark regions represent the PnBA immiscible phase. Since the ET/PMMA proceeded with reaction-induced immiscible behaviors,^{91,92} we rationally deduced that the white regions comprise mainly ET nearby excluded PMMA chains. Although we observed a small amount of PCL crystalline in DSC and XRD measurements, the gray regions are mainly composed of a miscible or at least partially miscible blend of ET/PCL which can be stained with a contrast in between (*i.e.*, gray color). A lamellar structure, however, appeared again for tBCP70%, with a mismatch to the volume fraction of PnBA ($f_{\text{PnBA}} = ca. 0.32$). The thermodynamic preference of the cylindrical microstructure could not be reached that might be ascribed to the kinetic limitations while curing. Fig. 9b2 reveals, interestingly, giant concentric-circular lamellae (CCL) with a radius of at least 3 μm . The interfacial curvature might have been driven by thermodynamic preference. To the best of our knowledge, this example is the first time such large-scale and uniform concentric circles have appeared within an ET matrix. In Fig. 10b, we observed a long-range-ordered lamellar structure, corresponding to q/q^* peaks of 1:2:3:5 with a periodic size of approximately 57.1 nm. Compared to the pure

tBCP results, the thickening of the periodic size was due to the incorporation of the ET within the PCL and PMMA regions. From the measurements of the tBCP50% composite in Fig. 9c and 10c, cylindrical morphology and the microstructure were acquired. In Fig. 9c, core/shell cylinders (CSC) with white domains located at the core and surrounded by gray domains were observed. These domains can have similar assignments according to the aforementioned tBCP70% composite. In Fig. 10c, the peaks were mainly composed of q/q^* peaks of 1: $\sqrt{3}$: $\sqrt{7}$ with a periodic size of approximately 38.8 nm. From the measurements of the tBCP30% composite in Fig. 9d and 10d, cylindrical morphology and the microstructure were also acquired. In Fig. 9d, a short core/shell cylinder (SCSC) was observed. According to the above cases, we can assign the compositions of these domains as white cores with ET/PMMA, dark shell with PnBA and gray surroundings with ET/PCL. In Fig. 10d, the broad peaks were mainly composed of q/q^* peaks of 1: $\sqrt{3}$: $\sqrt{7}$ with a periodic size of approximately 38.8 nm, but with a decrease in the degree of long-range order. We ascribe the broadened peaks to the coexisting microstructures of cylinders and spheres. In the corresponding TEM image (Fig. 9d), we can observe the presence of several spheres. From the measurements of the tBCP10% composite in Fig. 9e and 10e, spherical morphology and the microstructure were eventually acquired. In Fig. 9e, we observe that tBCP10% possessed solid sphere (S) morphology. In Fig. 10e, we observed broad peaks, which were correlated with a more disordered sphere morphology with dimensions of approximately 33.1 nm. Accordingly, the morphologies and the domain sizes of the composites detected using SAXS were similar to those analyzed using TEM, with only small deviations which might ascribed to the slight shrinkage under the vacuum environment for the TEM measurement. In summary, the TEM images revealed morphological differences and CCL–CSC–SCSC–S morphologies. Table 3 summarizes the TEM and SAXS characterization data.

Fig. 11 provides schematic representations of the microstructures of the ET/tBCP composites formed through the SA and RIMPS mechanisms, based on the TEM measurements. In the image of pure tBCP (*i.e.*, Fig. 9a), with dark and white contrast, we deduce that the dark stripe represented the phase-separated PnBA segments accompanied by a PCL-rich region on one side and a PMMA-rich region on the other side due to the PCL and PMMA segments are immiscible⁹⁶ and both appear with white contrast. As illustrated in Fig. 11a, the pure tBCP possessed a lamellar morphology, which was rational with respect to the volume fraction of the PnBA segment ($f_{\text{PnBA}} = 0.46$). For the ET/tBCP composites with dark, white, and gray contrast, we identified several regions consistent with the earlier images: (i) the originally phase-separated region of PnBA (stained as dark), (ii) the miscible or at least partially miscible region of ET/PCL and pure ET (presented as gray), and (iii) the reaction-induced immiscible region of ET/PMMA (stained as white). When an ET is mixed with a tBCP, the reaction-induced immiscible behavior has a critical effect governing the morphology of microphase separation. With a pre-formed microphase obtained through SA and a reorganized

Table 3 Microstructural characterization of the ET/tBCP composites

Sample	f_{PnBA}	TEM results		SAXS results	
		Morphology ^a	Domain size (nm)	Morphology ^a	Domain size (nm)
tBCP	0.46	L	42.8	L	46.5
tBCP70%	0.32	CCL	53.2	L	57.1
tBCP50%	0.23	CSC	34.4	C	38.8
tBCP30%	0.14	SCSC	32.1	C	38.8
tBCP10%	0.05	S	27.7	S	33.3

^a L: lamellae; CCL: concentric circle lamellae; CSC: core/shell cylinder; SCSC: short core/shell cylinder; C: cylinder; S: sphere.

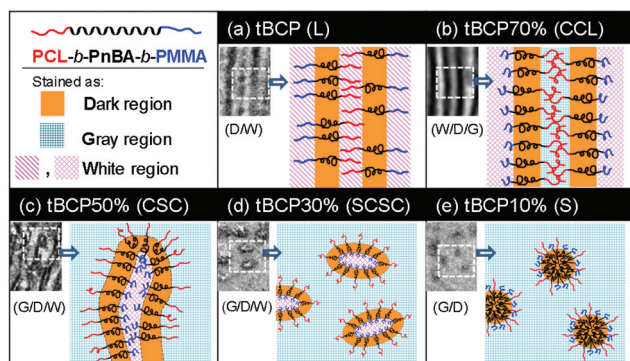


Fig. 11 Proposed microstructures of the ET/tBCP composites (D: dark; W: white; G: gray).

microphase obtained through RIMPS, this two-stage phase mechanism leads to the formation of highly compatible ET/tBCP nanocomposites. With an increase in the content of the ET, variations in the volume fractions of the phases (*i.e.*, $f_{(\text{ET}/\text{PCL})}$, $f_{(\text{ET}/\text{PMMA})}$, and f_{PnBA}) lead to interesting transitions with CCL–CSC–SCSC microstructures, as demonstrated in Fig. 11b–d, respectively. For tBCP10%, the excess of the ET can interact effectively with the tBCP nanoparticles and form a compact sphere having extended PCL chains and shrunken PMMA chains, as illustrated in Fig. 11e. Herein, we have demonstrated a facile and novel ET/tBCP system for the fabrication of hierarchical nanostructures, based on manipulation of kinetic and thermodynamic controls during the curing process.

4. Conclusions

We have synthesized a well-defined PCL–Br MI from a bifunctional initiator, mediated by the organocatalyst DPP, through ROP at 40 °C. We observed a linear first-order kinetic plot and linear growth of the MWs for the SARA ATRP chain extension of PCL–Br with nBA. We conducted a subsequent second-chain extension through HE ATRP, which overcame the challenge of low reactivity during polymerization. Thus, we have developed a mixed halide system that results in a linear first-order kinetic plot and linear growth of MWs. We obtained a well-defined tBCP, PCL₁₀₄–*b*–PnBA₁₇₂–*b*–PMMA₁₂₆ (M_n , NMR = 46 730; M_n , GPC = 56 600; PDI = 1.18). Through SAXS measure-

ments, we observed nano-sized homogeneity for the epoxy monomer and tBCP mixture, initially dictated by an SA mechanism. From FT-IR spectroscopic analysis, we detected a significant increase in the strength of intermolecular hydrogen bonding in the ET/tBCP composites. In DSC measurements of the ET/tBCP composites, we obtained two values of T_g (*ca.* –45 and +100 °C) that represented the excluded part of the PnBA and the immiscible part of the ET/PMMA, respectively. From TGA data, all of the composites possessed values of $T_{d5\%}$ of approximately 360 °C. Our results illustrate the merit of applying this ABC-type tBCP to hybridize with ET: to moderately retain the thermal properties with respect to those of the neat ET. On further examining the highly transparent ET/tBCP composites using TEM and SAXS, we found a lamellar morphology for the pure tBCP. With an increase in the amount of ET, we observed a transition among long-range-ordered CCL–CSC–SCSC morphologies by TEM. The microdomain sizes were approximately 30–60 nm. Thus, we have not only demonstrated the first successful synthesis of this well-defined high-MW ABC-type tBCP, PCL–*b*–PnBA–*b*–PMMA, but also demonstrated its effectiveness in the construction of long-range-ordered ET nanocomposites. These reproducible and stable ET nanocomposites have potential use in toughening systems, mesoporous materials, catalysis, separations, and lithography.

Conflicts of interest

There are no conflicts to declare.

Acknowledgements

The authors acknowledge the financial support from the Ministry of Science and Technology (MOST105-2218-E-005-004, MOST106-2218-E-005-021, and MOST105-2628-E-005-003-MY3).

References

- 1 N. Domun, H. Hadavinia, T. Zhang, T. Sainsbury, G. H. Liaghat and S. Vahid, *Nanoscale*, 2015, 7, 10294–10329.

- 2 S. J. Froggett, S. F. Clancy, D. R. Boverhof and R. A. Canady, *Part. Fibre Toxicol.*, 2014, **11**, 17.
- 3 M. A. Hillmyer, P. M. Lipic, D. A. Hajduk, K. Almdal and F. S. Bates, *J. Am. Chem. Soc.*, 1997, **119**, 2749–2750.
- 4 P. M. Lipic, F. S. Bates and M. A. Hillmyer, *J. Am. Chem. Soc.*, 1998, **120**, 8963–8970.
- 5 S. Jain and F. S. Bates, *Science*, 2003, **300**, 460–464.
- 6 L. Ruiz-Perez, G. J. Royston, J. P. A. Fairclough and A. J. Ryan, *Polymer*, 2008, **49**, 4475–4488.
- 7 W. C. Chu, L. Dai, J. K. Chen, C. F. Huang and S. W. Kuo, *J. Nanosci. Nanotechnol.*, 2016, **16**, 9085–9092.
- 8 C. F. Huang, S. W. Kuo, F. J. Lin, W. J. Huang, C. F. Wang, W. Y. Chen and F. C. Chang, *Macromolecules*, 2006, **39**, 300–308.
- 9 J. G. Li, Y. D. Lin and S. W. Kuo, *Macromolecules*, 2011, **44**, 9295–9309.
- 10 N. Hameed and Q. P. Guo, *Polymer*, 2008, **49**, 922–933.
- 11 H. Kosonen, J. Ruokolainen, P. Nyholm and O. Ikkala, *Polymer*, 2001, **42**, 9481–9486.
- 12 H. Kosonen, J. Ruokolainen, P. Nyholm and O. Ikkala, *Macromolecules*, 2001, **34**, 3046–3049.
- 13 W. C. Chu, J. G. Li and S. W. Kuo, *RSC Adv.*, 2013, **3**, 6485–6498.
- 14 W. C. Chu, J. G. Li, C. F. Wang, K. U. Jeong and S. W. Kuo, *J. Polym. Res.*, 2013, **20**, 272.
- 15 D. Hu and S. X. Zheng, *Polymer*, 2010, **51**, 6346–6354.
- 16 Y. Li and S. X. Zheng, *J. Polym. Sci., Part B: Polym. Phys.*, 2010, **48**, 1148–1159.
- 17 C.-C. Tsai, Z. Gan and S.-W. Kuo, *Polym. Chem.*, 2018, **9**, 3684–3693.
- 18 F. L. Meng, S. X. Zheng, H. Q. Li, Q. Liang and T. X. Liu, *Macromolecules*, 2006, **39**, 5072–5080.
- 19 R. B. Grubbs, J. M. Dean, M. E. Broz and F. S. Bates, *Macromolecules*, 2000, **33**, 9522–9534.
- 20 R. B. Grubbs, J. M. Dean and F. S. Bates, *Macromolecules*, 2001, **34**, 8593–8595.
- 21 J. M. Dean, R. B. Grubbs, W. Saad, R. F. Cook and F. S. Bates, *J. Polym. Sci., Part B: Polym. Phys.*, 2003, **41**, 2444–2456.
- 22 J. M. Dean, N. E. Verghese, H. Q. Pham and F. S. Bates, *Macromolecules*, 2003, **36**, 9267–9270.
- 23 Q. P. Guo, J. M. Dean, R. B. Grubbs and F. S. Bates, *J. Polym. Sci., Part B: Polym. Phys.*, 2003, **41**, 1994–2003.
- 24 V. Rebizant, V. Abetz, F. Tournilhac, F. Court and L. Leibler, *Macromolecules*, 2003, **36**, 9889–9896.
- 25 V. Rebizant, A. S. Venet, F. Tournilhac, E. Girard-Reydet, C. Navarro, J. P. Pascault and L. Leibler, *Macromolecules*, 2004, **37**, 8017–8027.
- 26 N. Hameed, Q. P. Guo, Z. G. Xu, T. L. Hanley and Y. W. Mai, *Soft Matter*, 2010, **6**, 6119–6129.
- 27 E. Serrano, A. D. Martin, A. Tercjak, J. A. Pomposo, D. Mecerreyes and I. Mondragon, *Macromol. Rapid Commun.*, 2005, **26**, 982–985.
- 28 E. Serrano, A. Tercjak, C. Ocando, M. Larranaga, M. D. Parellada, S. Corona-Galvan, D. Mecerreyes, N. E. Zafeiropoulos, M. Stamm and I. Mondragon, *Macromol. Chem. Phys.*, 2007, **208**, 2281–2292.
- 29 N. V. Salim, N. Hameed, B. L. Fox and T. L. Hanley, *Macromolecules*, 2015, **48**, 8337–8345.
- 30 Q. P. Guo, P. Figueiredo, R. Thomann and W. Gronski, *Polymer*, 2001, **42**, 10101–10110.
- 31 J. Mijovic, M. Z. Shen, J. W. Sy and I. Mondragon, *Macromolecules*, 2000, **33**, 5235–5244.
- 32 J. M. Dean, P. M. Lipic, R. B. Grubbs, R. F. Cook and F. S. Bates, *J. Polym. Sci., Part B: Polym. Phys.*, 2001, **39**, 2996–3010.
- 33 J. X. Wu, Y. S. Thio and F. S. Bates, *J. Polym. Sci., Part B: Polym. Phys.*, 2005, **43**, 1950–1965.
- 34 Y. S. Thio, J. X. Wu and F. S. Bates, *Macromolecules*, 2006, **39**, 7187–7189.
- 35 I. A. Zucchi, M. J. Galante and R. J. J. Williams, *Polymer*, 2005, **46**, 2603–2609.
- 36 T. Fine, F. Lortie, L. David and J. P. Pascault, *Polymer*, 2005, **46**, 6605–6613.
- 37 J. Liu, H. J. Sue, Z. J. Thompson, F. S. Bates, M. Dettloff, G. Jacob, N. Verghese and H. Pham, *Macromolecules*, 2008, **41**, 7616–7624.
- 38 Z. J. Thompson, M. A. Hillmyer, J. Liu, H. J. Sue, M. Dettloff and F. S. Bates, *Macromolecules*, 2009, **42**, 2333–2335.
- 39 J. Liu, Z. J. Thompson, H. J. Sue, F. S. Bates, M. A. Hillmyer, M. Dettloff, G. Jacob, N. Verghese and H. Pham, *Macromolecules*, 2010, **43**, 7238–7243.
- 40 P. C. Sun, Q. Q. Dang, B. H. Li, T. H. Chen, Y. N. Wang, H. Lin, Q. H. Jin, D. T. Ding and A. C. Shi, *Macromolecules*, 2005, **38**, 5654–5667.
- 41 Q. P. Guo, R. Thomann, W. Gronski and T. Thurn-Albrecht, *Macromolecules*, 2002, **35**, 3133–3144.
- 42 H. Kishi, Y. Kunimitsu, J. Imade, S. Oshita, Y. Morishita and M. Asada, *Polymer*, 2011, **52**, 760–768.
- 43 H. Kishi, Y. Kunimitsu, Y. Nakashima, T. Abe, J. Imade, S. Oshita, Y. Morishita and M. Asada, *EXPRESS Polym. Lett.*, 2015, **9**, 23–35.
- 44 M. Asada, S. Oshita, Y. Morishita, Y. Nakashima, Y. Kunimitsu and H. Kishi, *Polymer*, 2016, **105**, 172–179.
- 45 H. Kishi, Y. Kunimitsu, Y. Nakashima, J. Imade, S. Oshita, Y. Morishita and M. Asada, *EXPRESS Polym. Lett.*, 2017, **11**, 765–777.
- 46 F. L. Meng, S. X. Zheng, W. Zhang, H. Q. Li and Q. Liang, *Macromolecules*, 2006, **39**, 711–719.
- 47 F. L. Meng, F. P. Yi and S. X. Zheng, *J. Macromol. Sci., Part B: Phys.*, 2008, **47**, 450–462.
- 48 S. S. Chen, B. Chen, J. S. Fan and J. C. Feng, *ACS Sustainable Chem. Eng.*, 2015, **3**, 2077–2083.
- 49 S. Ritzenthaler, F. Court, E. Girard-Reydet, L. Leibler and J. P. Pascault, *Macromolecules*, 2003, **36**, 118–126.
- 50 S. Ritzenthaler, F. Court, L. David, E. Girard-Reydet, L. Leibler and J. P. Pascault, *Macromolecules*, 2002, **35**, 6245–6254.
- 51 W. C. Fan, L. Wang and S. X. Zheng, *Macromolecules*, 2009, **42**, 327–336.
- 52 W. C. Fan, L. Wang and S. X. Zheng, *Macromolecules*, 2010, **43**, 10600–10611.

- 53 H. L. Cong, L. Li and S. X. Zheng, *Polymer*, 2014, **55**, 1190–1201.
- 54 H. L. Cong, L. Li and S. X. Zheng, *Polymer*, 2015, **80**, 146–158.
- 55 W. H. Qian, X. M. Song, C. Feng, P. C. Xu, X. Jiang, Y. J. Li and X. Y. Huang, *Polym. Chem.*, 2016, **7**, 3300–3310.
- 56 B. B. Xu, C. Feng, J. H. Hu, P. Shi, G. X. Gu, L. Wang and X. Y. Huang, *ACS Appl. Mater. Interfaces*, 2016, **8**, 6685–6692.
- 57 W. H. Qian, T. Song, M. Ye, P. C. Xu, G. L. Lu and X. Y. Huang, *Polym. Chem.*, 2017, **8**, 4098–4107.
- 58 B. B. Xu, C. Feng and X. Y. Huang, *Nat. Commun.*, 2017, **8**, 333.
- 59 B. B. Xu, Y. J. Liu, X. W. Sun, J. H. Hu, P. Shi and X. Y. Huang, *ACS Appl. Mater. Interfaces*, 2017, **9**, 16517–16523.
- 60 X. Jiang, Y. Deng, W. B. Liu, Y. J. Li and X. Y. Huang, *Polym. Chem.*, 2018, **9**, 184–192.
- 61 A. Hirao and S. Nakahama, *Acta Polym.*, 1998, **49**, 133–144.
- 62 N. Hadjichristidis, M. Pitsikalis, S. Pispas and H. Iatrou, *Chem. Rev.*, 2001, **101**, 3747–3792.
- 63 S. Ito, R. Goseki, T. Ishizone and A. Hirao, *Polym. Chem.*, 2014, **5**, 5523–5534.
- 64 M. Sawamoto, *Prog. Polym. Sci.*, 1991, **16**, 111–172.
- 65 R. Jordan and A. Ulman, *J. Am. Chem. Soc.*, 1998, **120**, 243–247.
- 66 Y. Yagci and I. Reetz, *Prog. Polym. Sci.*, 1998, **23**, 1485–1538.
- 67 W. A. Braunecker and K. Matyjaszewski, *Prog. Polym. Sci.*, 2007, **32**, 93–146.
- 68 K. Matyjaszewski, *ACS Symp. Ser.*, 2009, **1023**, 3–14.
- 69 C. J. Hawker, A. W. Bosman and E. Harth, *Chem. Rev.*, 2001, **101**, 3661–3688.
- 70 M. Kamigaito, T. Ando and M. Sawamoto, *Chem. Rev.*, 2001, **101**, 3689–3745.
- 71 G. Moad, E. Rizzardo and S. H. Thang, *Polymer*, 2008, **49**, 1079–1131.
- 72 C.-F. Huang, W. Chen, T. P. Russell, A. C. Balazs, F.-C. Chang and K. Matyjaszewski, *Macromol. Chem. Phys.*, 2009, **210**, 1484–1492.
- 73 C. W. Bielawski and R. H. Grubbs, *Prog. Polym. Sci.*, 2007, **32**, 1–29.
- 74 N. E. Kamber, W. Jeong, R. M. Waymouth, R. C. Pratt, B. G. G. Lohmeijer and J. L. Hedrick, *Chem. Rev.*, 2007, **107**, 5813–5840.
- 75 T. Yokozawa and A. Yokoyama, *Chem. Rev.*, 2009, **109**, 5595–5619.
- 76 Y. Z. Zhang, Y. Wang and K. Matyjaszewski, *Macromolecules*, 2011, **44**, 683–685.
- 77 P. Kryszewski, Y. Wang, K. Matyjaszewski and S. Harrison, *Macromolecules*, 2016, **49**, 2977–2984.
- 78 K.-Y. Lai, Y.-S. Huang, C.-Y. Chu and C.-F. Huang, *Polymer*, 2018, **137**, 385–394.
- 79 K. Matyjaszewski, D. A. Shipp, J. L. Wang, T. Grimaud and T. E. Patten, *Macromolecules*, 1998, **31**, 6836–6840.
- 80 B. Dufour, K. Koynov, T. Pakula and K. Matyjaszewski, *Macromol. Chem. Phys.*, 2008, **209**, 1686–1693.
- 81 K. Matyjaszewski, D. A. Shipp, G. P. McMurtry, S. G. Gaynor and T. Pakula, *J. Polym. Sci., Part A: Polym. Chem.*, 2000, **38**, 2023–2031.
- 82 C.-F. Huang, J.-K. Chen, T.-Y. Tsai, Y.-A. Hsieh and K.-Y. A. Lin, *Polymer*, 2015, **72**, 395–405.
- 83 Y.-M. Han, H.-H. Chen and C.-F. Huang, *Polym. Chem.*, 2015, **6**, 4565–4574.
- 84 R. Kakuchi, Y. Tsuji, K. Chiba, K. Fuchise, R. Sakai, T. Satoh and T. Kakuchi, *Macromolecules*, 2010, **43**, 7090–7094.
- 85 K. Makiguchi, T. Satoh and T. Kakuchi, *Macromolecules*, 2011, **44**, 1999–2005.
- 86 K. Makiguchi, Y. Ogasawara, S. Kikuchi, T. Satoh and T. Kakuchi, *Macromolecules*, 2013, **46**, 1772–1782.
- 87 W. Tang, Y. Kwak, W. Braunecker, N. V. Tsarevsky, M. L. Coote and K. Matyjaszewski, *J. Am. Chem. Soc.*, 2008, **130**, 10702–10713.
- 88 Z. G. Xu and S. X. Zheng, *Polymer*, 2007, **48**, 6134–6144.
- 89 L. Konczol, W. Doll, U. Buchholz and R. Mulhaupt, *J. Appl. Polym. Sci.*, 1994, **54**, 815–826.
- 90 S. Y. Wu, S. H. Peng, N. Hameed, Q. P. Guo and Y. W. Mai, *Soft Matter*, 2012, **8**, 688–698.
- 91 M. J. Galante, J. Borrajo, R. J. J. Williams, E. Girard-Reydet and J. P. Pascault, *Macromolecules*, 2001, **34**, 2686–2694.
- 92 E. M. Woo and M. N. Wu, *Polymer*, 1996, **37**, 2485–2492.
- 93 Z. G. Xu and S. Zheng, *Macromolecules*, 2007, **40**, 2548–2558.
- 94 S. Gazit and J. P. Bell, *ACS Symp. Ser.*, 1983, **221**, 55–67.
- 95 X. F. Wang, H. B. Zhao, L. S. Turng and Q. Li, *Ind. Eng. Chem. Res.*, 2013, **52**, 4939–4949.
- 96 G. A. Abraham, A. Gallardo, A. Motta, C. Migliaresi and J. San Roman, *Macromol. Mater. Eng.*, 2000, **282**, 44–50.